2008

Simian Immunodeficiency Virus–Induced Intestinal Cell Apoptosis Is the Underlying Mechanism of the Regenerative Enteropathy of Early Infection

Qingsheng Li
University of Minnesota, Minneapolis, qli4@unl.edu

Jacob D. Estes
University of Minnesota, Minneapolis, estesj@mail.nih.gov

Lijie Duan
University of Minnesota, Minneapolis

Jose Jessurun
University of Minnesota, Minneapolis

Stefan Pambuccian
University of Minnesota, Minneapolis

See next page for additional authors

Published in *The Journal of Infectious Diseases* 197 (2008), pp. 420–429. doi: 10.1086/525046

Submitted April 9, 2007; accepted May 21, 2007; published online January 16, 2008.

Simian Immunodeficiency Virus–Induced Intestinal Cell Apoptosis Is the Underlying Mechanism of the Regenerative Enteropathy of Early Infection

Qingsheng Li,[1] Jacob D. Estes,[1] Lijie Duan,[1] Jose Jessurun,[2] Stefan Pambuccian,[2] Colleen Forster,[3] Stephen Wietgrefe,[1] Mary Zupancic,[1] Timothy Schacker,[4] Cavan Reilly,[5] John V. Carlis,[6] and Ashley T. Haase[1]

University of Minnesota, Minneapolis:
1. Department of Microbiology
2. Department of Laboratory Medicine and Pathology
3. Neuropathology Laboratory, Department of Laboratory Medicine and Pathology
4. Division of Infectious Diseases, Department of Medicine, Medical School
5. Division of Biostatistics, School of Public Health
6. Department of Computer Science and Engineering, Institute of Technology

Corresponding author – Ashley T. Haase, Dept. of Microbiology, University of Minnesota, MMC 196, 420 Delaware St. SE, Minneapolis, MN 55455; email haase001@umn.edu

Abstract

The enteropathic manifestations of the human immunodeficiency virus (HIV) and the simian immunodeficiency virus (SIV) in late infection are usually due to infection by other microbes, but in early infection the viruses themselves cause an enteropathy by heretofore undetermined mechanisms. Here we report that SIV induces massive apoptosis of intestinal epithelial cells lining the small and large bowel, thus identifying apoptosis as the driving force behind the regenerative pathology of early infection. We found that apoptosis of gut epithelium paralleled the previously documented apoptosis and massive depletion of CD4 T cells in gut lamina propria, triggered by established mechanisms of gut epithelial cell apoptosis and, at peak, possibly by virus interactions with GPR15/Bob, an intestinal epithelial cell–associated alternative coreceptor for SIV and HIV-1. Apoptosis in early SIV infection is thus the common theme of the pathological processes that quickly afflict the innate as well as adaptive arms of the gut immune system.

Diarrhea, malabsorption, and weight loss, enteropathic manifestations of HIV type 1 (HIV-1) [1–4], and simian immunodeficiency virus (SIV) infections [5–7] are usually the result of concurrent infection by other viruses, bacteria, and protozoa in the later stages of infection. However, both HIV-1 [8] and SIV can themselves, in the absence of other enteric pathogens, cause malabsorption and histopatholgical changes in the gut that are detectable as early as the end of the second week of SIV infection [6, 7]. The underlying mechanism of these earlystage-HIV and -SIV enteropathies are unknown, but the increased expression of cell-cycle genes [9, 10] and pathological changes of regenerative villous atrophy [5, 7, 11] point to infection-induced increases in turnover of gut epithelium.

We sought the antecedent causes of the enteropathy and increased turnover of gut epithelium in tissues collected in the course of published studies [12] of the SIVnonhuman- primate (rhesus macaque) model of HIV-1 vaginal transmission and early infection. We reasoned that these tissues might provide an opportunity to discover virus-induced mechanisms of increased turnover and enteropathy in the time frame when they might be the most apparent, between 7 days postinoculation (dpi) and 10–14 dpi. The former is the time infection had disseminated from the vaginal site of inoculation to gutassociated and other lymphatic tissues, whereas the latter is the peak period of viral replication in the gut and throughout the lymphatic tissues and the time at which evidence of increased turnover of gut epithelium had been previously documented [7, 9–11]. We now report that, within this short period, there is massive apoptosis and an associated increase in proliferation of gut epithelium, which identify apoptosis of gut epithelium as the underlying mechanism of the regenerative villous atrophy that characterizes the gut pathology of early infection.

Table 1. Information on the animals and status of tissues.

Day(s) postinoculation[a]	Cervical/ vaginal infection	Gut infection	Gut lamina propria CD4 T cells	
			Depletion	Apoptosis
0, 2	–	–	–	–
4	+	–	–	–
7, 8	+	+	+	3+
13, 14	+	3+	3+	±
21	+	2+	3+	±
28	±	+	3+	±

Key: –, not detected; +, detected on scale of 1–3; ±, detected at low frequency. Data are from Miller et al. [12] and Li et al. [13].

a. Infection of tissues was determined by detection of simian immunodeficiency virus RNA^+ cells, by in situ hybridization.

Materials and Methods

Gut tissues from SIV-infected animals. Colon and small-bowel tissues were obtained at necropsy 1–28 days after adult female rhesus macaques (*Macacca mulatta*) had been inoculated intravaginally twice the same day with 1×10^5 of 50% tissueculture infectious dose of either SIVmac251 or SIVmac239, as described by Miller et al. [12] and summarized in table 1. Tissues were fixed in paraformaldehyde or Streck's Tissue Fixative before being embedded in paraffin.

Immunohistochemistry. Tissue sections (5–8 μm) fixed in either paraformaldehyde or Streck's Tissue Fixative were rehydrated in deionized distilled water and blocked for endogenous peroxidase activity by being immersed in 3% H_2O_2 in methanol for 30 min. For antigen retrieval, slides were incubated in either citrate buffer (10 mmol/L, pH 6.0), EDTA (1 mmol/L, pH 8.0), EDTA Decloaker (Biocare Medical), or Reveal buffer (Biocare Medical) for 20 min at 95°C–98°C, and, after cooling for 20 min, the slides were immersed in 3% normal serum in TNB (TNB blocking buffer, 0.1 mol/L Tris-HCl, pH 7.5; 0.15 mol/L NaCl; 0.5% blocking reagent [Dupont]) for 30 min and in BACKGROUND SNIPER (Biocare Medical) for 10 min–1 h. The sections were then incubated overnight at 4°C in a humidified chamber with primary antibodies (table 2) diluted in either 10% BACKGROUND SNIPER or, as a negative control, isotype control immunoglobulin. After being rinsed, the sections were developed by staining, according to the manufacturer's instructions, in one of the following systems: biotin-free mouse DakoCytomation EnVision+ System-HRP (Dako), MACH-3 mouse–horseradish peroxidase (HRP) polymer (Biocare Medical), MACH-3 rabbit-probe HRP polymer (Biocare Medical), MACH-3 mouse-probe alkaline phosphatase polymer (Biocare Medical) and HRP substrate diaminobenzidine (DAB), or alkaline-phosphatase substrate Vulcan Fast Red (Biocare Medical). The sections were then counterstained with hematoxylin (Biocare Medical), for the Fast Red substrate, and Harris hematoxylin (Surgipath Medical), for the DAB substrate. All immunohistochemical (and immunofluorescent) staining was shown to be specific, on the basis of the lack of staining with the isotype control. For the antibodies used, sources, dilutions, and other details, see table 2.

Immunofluorescence and confocal microscopy. As has been described by Li et al. [13], sections were stained with primary antibodies overnight at 4°C, were washed in PBS-Tween20 (0.05% v/v), and incubated, for 1 h at room temperature, with donkey secondary antibodies with minimal cross-reactivity that were conjugated with Alexa 488 (green) or 555 (red). Cell nuclei were counterstained blue withTOTO-3.ABio-RadMRC1000 confocal microscope was used to collect, at wavelengths specific for each fluorophore, confocal images at 600× or 1200× magnification, by acquiring, at every time point analyzed, the brightest point projection from at least 12–18 randomly selected regions of the small and large bowel. For every image collected, each fluorescence channel was sequentially acquired, binary images were imported into Adobe Photoshop CS Photoshop, were converted into red/green/blue color images, and were merged to generate either dual- or triple-labeled images. To allow better visualization of the GPR15/Bob receptor translocation and alterations, some images not showing nuclear staining are also shown.

In situ hybridization. SIV RNA was detected, by in situ hybridization, in paraformaldehyde-fixed and paraffin-embedded tissues, as described by Li et al. [13]. In brief, 6–8 μm sections were cut and adhered to slides treated with 3-aminopropyltrioxysilane. After deparaffinization in xylene, rehydration in PBS, and permeabilization by treating the sections with HCl, digitonin, and proteinase K, the sections were acetylated and hybridized to ^{35}S-labeled SIVspecific riboprobes. After being washed and digested with ribonucleases, the sections were coated with nuclear-track emulsion, were exposed and developed, and were counterstained with Wright.

Quantification of gut epithelial cell apoptosis and proliferation. We quantified apoptosis and proliferation by using an approach similar to that described by Holubec et al. [14]. Images of colon tissue immunohistochemically stained to detect cleaved cytokeratin 18 or Ki67 and counterstained with hematoxylin were randomly captured by use of Scion visiCapture software (version 1.3) and an Olympus BX60 microscope (20x/numeric aperture 0.70) coupled with a Scion Color IEEE-1394 Camera (Scion). Cleaved $CK18^+$ gut epithelial cells and total gut epithelial nuclei in 30 fields at 200× magnification were enumerated manually and independently by 2 investigators using Adobe Photoshop CS2. Apoptosis was expressed as the mean percentage of cleaved $CK18^+$ cells and nuclei counted. Colonic proliferating $Ki67^+$ cells were similarly quantified in crypts, in which the bases, middle portions, and tops were in the same focal plane.

Table 2. Details on antibodies used. The table is available following page 429.

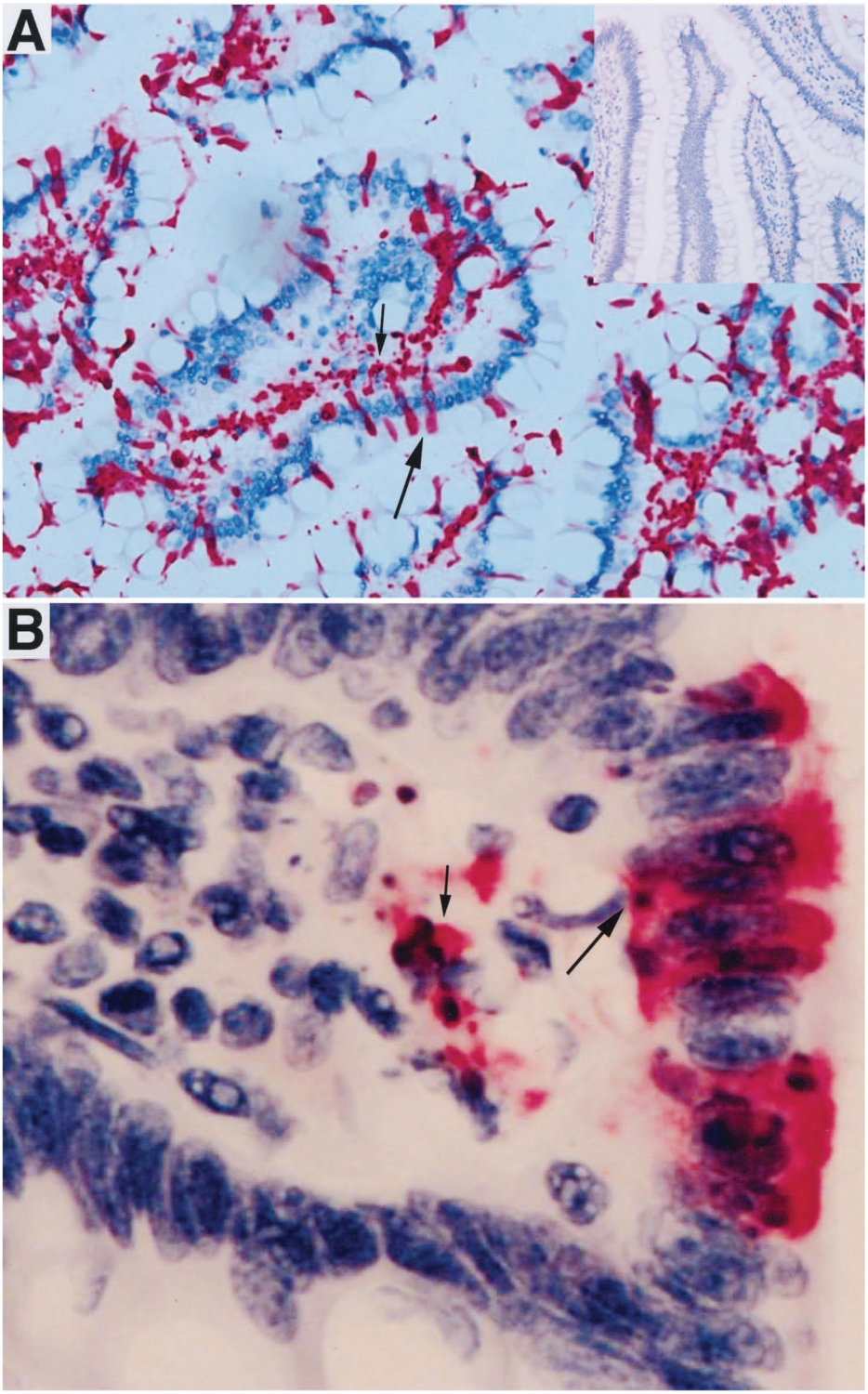

Figure 1. Apoptosis of gut epithelial cells and lamina propria cells in small and large bowel, in early simian immunodeficiency virus infection. Activated caspase-3 as a marker of apoptosis was detected immunohistochemically by use of Vulcan Fast Red substrate. In panel *A,* the larger arrow indicates one of several red-stained apoptotic gut epithelial cells lining a cross-section of jejunal villi at the onset of viral replication in gut, and the smaller arrow indicates one of many red-stained activated caspase-3$^+$ apoptotic cells in the lamina propria, which elsewhere have been shown to be effector memory CD4$^+$ T cells [13]. The inset shows the negligible staining in a section of jejunum from an uninfected animal. Original magnification, ×200. In panel *B,* the large arrow indicates one of several apoptotic gut epithelial cells lining the colon, and the small arrow indicates apoptotic lamina propria cells at the onset of viral replication in gut. Original magnification, ×400.

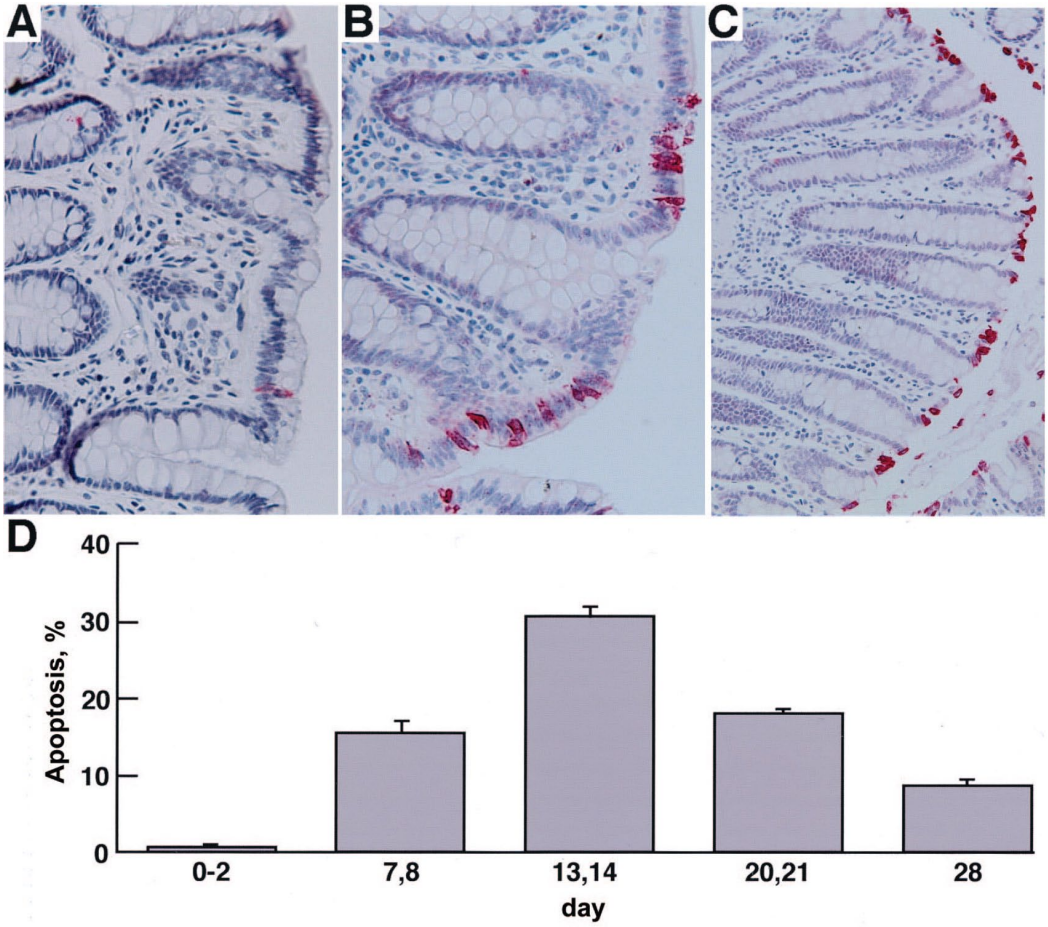

Figure 2. Time course of increased gut epithelial cell apoptosis in the large bowel. *A–C,* Apoptotic epithelial cells stained red with antibodies to cleaved cytokeratin 18, a specific marker for epithelial cell apoptosis, and Vulcan Fast Red substrate. Note the increasing number of red-staining apoptotic cells lining the bowel, in an uninfected animal *(A)* and in an animal at the onset *(B)* and peak *(C)* of gut infection. Original magnifications, ×200. *D,* Percentage of apoptotic gut epithelial cells in large bowel, determined as described in Materials and Methods, in 2 animals per time point, for the indicated days after intravaginal inoculation. Days 0 and 2 (0–2) are, respectively, before inoculation and before spread of infection to gut; days 7 and 8 are the initial phase of gut infection, days 13 and 14 are the broad peak of replication, and days 20, 21, and 28 are the decline phase, in return to set-point levels. Error bars indicate SEs.

Statistical tests. To examine the overall effect, at various weeks postinfection, on the levels of cytokeratin 18 and Ki67, we fit an analysis-of-variance model and used the *F* statistic to test for an effect of time (with weeks postinfection being treated as a factor). This method allows us to investigate the effect of time without having to assume some form for the relationship (such as linear) between levels and time. To then test for differences between baseline levels and those at specific days, we used the 2-sample *t* test (with equal variances). To control the overall significance level for each response of interest, a Bonferonni adjustment was used for these *t* tests.

Results

Gut epithelial cell apoptosis in early SIV infection. Elsewhere, we already had shown that, at 7–14 dpi, there was massive depletion of memory $CD4^+$ T cells and that this coincided with commensurate increases in apoptosis of lamina propria$CD4^+$ T cells [13], as is illustrated, in figure 1, by the large number of activated caspase 3^+ cells in small-bowel lamina propria at 8 dpi, a result supporting our previously reported conclusion [13] that apoptosis of $CD4^+$ T cells contributed significantly to $CD4^+$ T cell depletion in the gut. However, as is evident in figure 1, we also observed focal increases in activated caspase-3^+ apoptotic gut epithelial cells in both the small and large bowel (figure 1*A*and 1*B*), which suggested a new hypothesis: apoptosis of gut epithelium is the mechanism underlying the regenerative enteropathy of early infection.

To test this hypothesis, we quantified apoptosis of gut epithelium over the course of early infection, with the same tissues and time frame that we had used to document apoptosis of lamina propria $CD4^+$ T cells (table 1 and [12, 13]). As predicted by the hypothesis, we found large increases in activated caspase 3^+ gut epithelium lining the small and large bowel. Increased apoptosis was detectable in the exponential phase (7 dpi) of viral replication in the

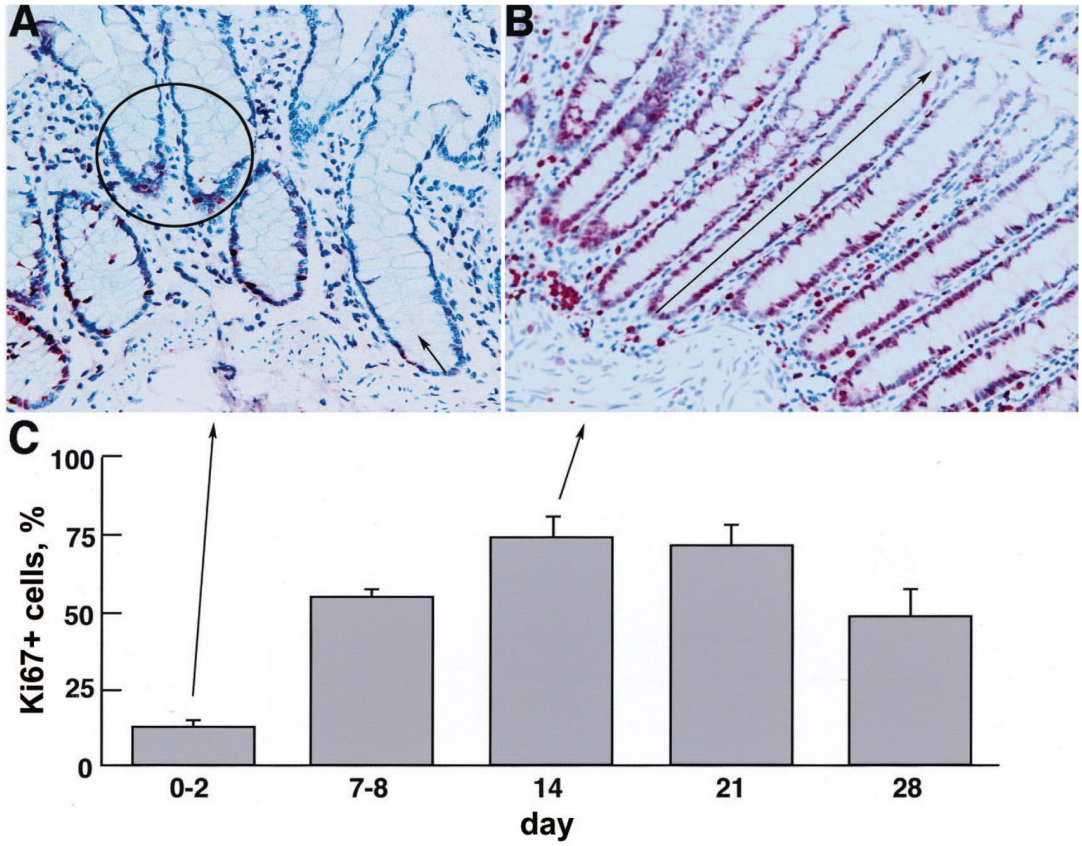

Figure 3. Increased proliferation of gut epithelial cells. Cycling cells were detected immunohistochemically by use of antibodies to Ki67 and Vulcan Fast Red substrate. Sections were counterstained blue with Biocare hematoxylin. Before gut infection (day 0) *(A)*, most of the red-stained proliferating Ki67$^+$ gut epithelial cells are either close to the base of the colonic crypts *(encircled)* or extend only a short way toward the top *(short arrow)*. At peak replication and gut epithelial cell apoptosis *(B)*, increased numbers of Ki67$^+$ gut epithelial cells extend from the base to nearly the tops of the crypts *(long arrow)*. Original magnification, ×200. *C*, Percentage of colonic Ki67$^+$ gut epithelial cells, determined as described in Materials and Methods, in animals at the time points shown, corresponding to animals described in figure 2. Increased proliferation was detectable at 7 days postinoculation (dpi), peaked at 14 dpi, and remained elevated at 28 dpi, the last time point of examination. Arrows point to the corresponding images in panels *A* and *B*.

gut, peaked at day 14 dpi, in parallel with peak viral replication, and then decreased by 28 dpi, the last time point examined in these studies [12]. We confirmed the activated caspase-3 results by using antibodies to cleaved cytokeratin 18, a specific marker for epithelial cell apoptosis [14], in colon-tissue sections stained with this antibody. Figure 2*A*–2*C* shows the increases in apoptosis of gut epithelium at 7 and 14 dpi, compared with apoptosis in an uninfected animal. We quantified the changes by using this marker in apoptotic epithelial cells in the colons (figure 2*D*) of 2 animals before detection of SIV-infected cells in the gut (i.e., at 0–2 dpi) and in 8 animals after gut infection (2 animals each in the exponential, peak, and decline phases [2 animals at days 20/21 and 2 animals at day 28] of viral replication in the gut tissues) [13]. The percentage of apoptotic epithelial cells lining the colon at 7–8 dpi was 15-fold higher than either that in an uninfected animal or that in an infected animal before gut infection, was 30-fold higher at the peak (i.e., at 14 dpi), and was still 8-fold higher at 28 dpi. There was remarkably little interanimal variation (note that the SEs for animals examined 1 or 2 days apart were small), which attested to the reproducibility of the process, and all the increases were highly statistically significant: $P = 5.6 \times 10^{-6}$ overall and $P = .004$ when the percentage before infection of gut was compared with that at 28 dpi.

Gut epithelial cell proliferation and gut pathology in early SIV infection. These increases suggested that, to maintain mucosal integrity, gut epithelial cell apoptosis might drive a compensatory increase in proliferation, as an exaggeration of a normal homeostatic mechanism in the gut, in which the integrity of the mucosal barrier is maintained by balancing the loss of apoptotic epithelial cells at the tops of the crypts by replacement through division of stem cells at the bases of the crypts [15]. We indeed documented increases in proliferation of gut epithelium that are consistent with a compensatory response to increased apoptosis. Using Ki67 as a marker for cell proliferation, we detected increased numbers of Ki67$^+$ gut epithelial cells, and they continued to increase in parallel with gut epithelial apoptosis, peaking at highly significant ($P > .001$) levels, >3-fold higher than either those in an uninfected animal or those in an infected animal before gut infection. In

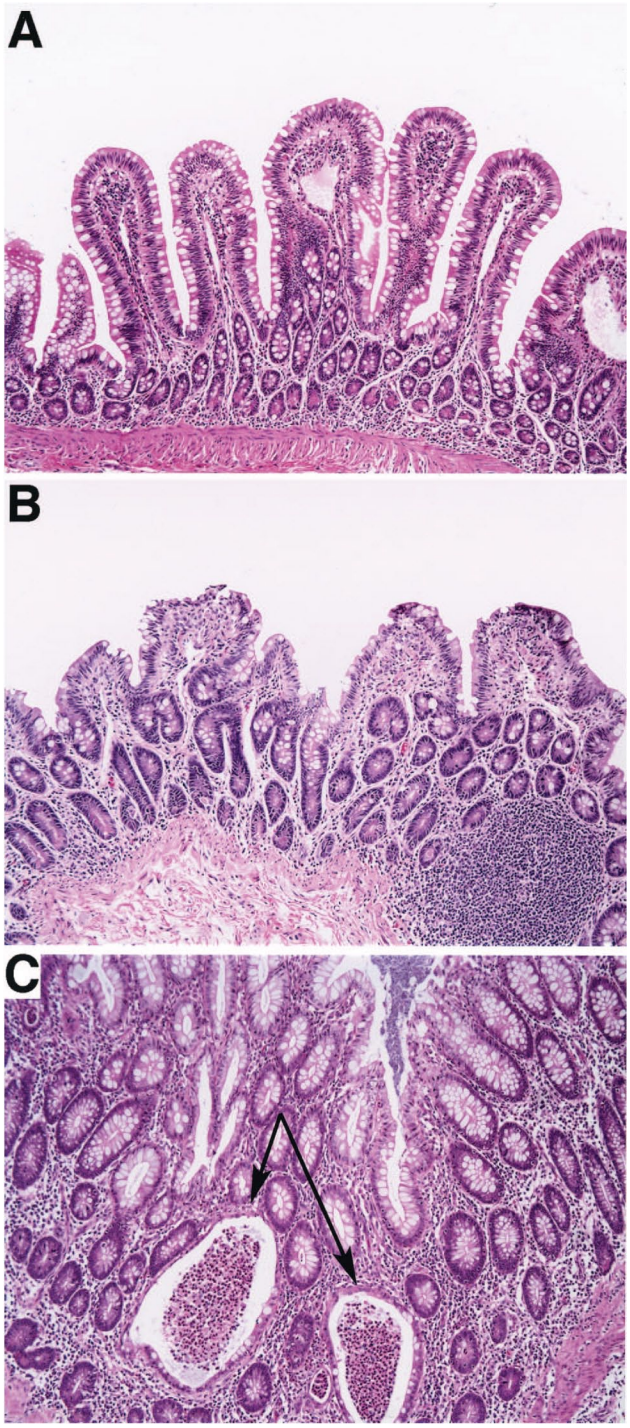

Figure 4. Gut pathology. Sections of jejunum stained with hematoxylin and eosin, from animals before *(A)* and 28 dpi *(B)* infection, showing the shortened villi. *C*, 2 microabscesses with neutrophilic infiltrates *(arrows)* in large bowel at 28 dpi. Original magnifications, ×100.

addition, the Ki67$^+$ gut epithelial cells were not confined to the bases but extended to the tops of the colonic crypts (figure 3*A*–3*C*).

The increased proliferation was associated with the histopathological changes in acute SIV infection of regenerative villous atrophy in the small bowel that have been described elsewhere [5, 7, 11]. Villous atrophy was already detectable at the second week of infection but was most prominent at 28 dpi (figure 4*A*– 4*C*); at that time, there was additional evidence of pathology in 1 animal in which we found multiple microabscesses with neutrophilic infiltrates (figure 4*C*).

Gut epithelial cell apoptosis: possible mechanisms. We investigated 4 mechanisms by which SIV infection and associated immune activation might induce gut epithelial cell apoptosis. First, we found that productive infection of gut epithelial cells is not likely to be the mechanism, because the only cells in which we detected SIVRNAby in situ hybridization were mononuclear cells (MNCs) in the lamina propria and lymphoid follicles (figure 5*A*), cells that we had elsewhere shown to be memory CD4$^+$ T cells [13]. Second, because increased expression of Fas in enterocytes and Fas-L by intraepithelial or lamina propria lymphocytes can induce gut epithelial cell apoptosis [16, 17], we assessed Fas and Fas-L expression and found that, at the onset of increased gut epithelial cell apoptosis, there was a correlation between focal increases in expression of Fas in enterocytes and lamina propria lymphocytes (figure 5*B*) and Fas-L expression in lamina propria lymphocytes (figure 5*C*), a correlation that is consistent with this second mechanism. However, such a mechanism could not account for the peak of gut epithelial cell apoptosis at 14 dpi, because, by that time, Fas-L$^+$ lamina propria lymphocytes had been largely depleted and Fas$^+$ gut epithelial cells were no longer detectable (not shown). Third, because proinflammatory cytokine tumor-necrosis factor (TNF)–α and interferon (IFN)–γ induce gut epithelial cell apoptosis in vitro [18, 19], we investigated their expression.Wefound that, at the onset of increased gut epithelial cell apoptosis, there were also increased numbers of cells positive for TNF-α (figure 5*D*) and IFN-γ (not shown), findings that are consistent with both a contribution to the initial increases in gut epithelial cell apoptosis and the previously documented increased expression of IFN-γ and TNF-α mRNA in gut and other tissues from these animals [20]. However, again, at the peak of gut epithelial cell apoptosis, we did not detect TNF-α$^+$ cells by immunohistochemical staining (figure 5*E*), a result that is consistent with the results of analyses of cytokinemRNAlevels in these animals, in which peak gut epithelial cell apoptosis occurs at a time when TNF-α and IFN-γ mRNAs have been reported to be at their lowest level in the gut [20]. Thus, established mechanisms of gut epithelial apoptosis may play a role in the initial increases in gut epithelial cell apoptosis but cannot account for its peak level.

Gut epithelial cell apoptosis coincides with viral deposition at the basal surfaces of gut epithelial cells, and transcytosis and shedding of GPR15/Bob. Peak gut epithelial cell apoptosis coincided with visible interactions between virus and GPR15/ Bob, an alternative coreceptor for SIV [21] and HIV [22] and a mediator of CD4-independent

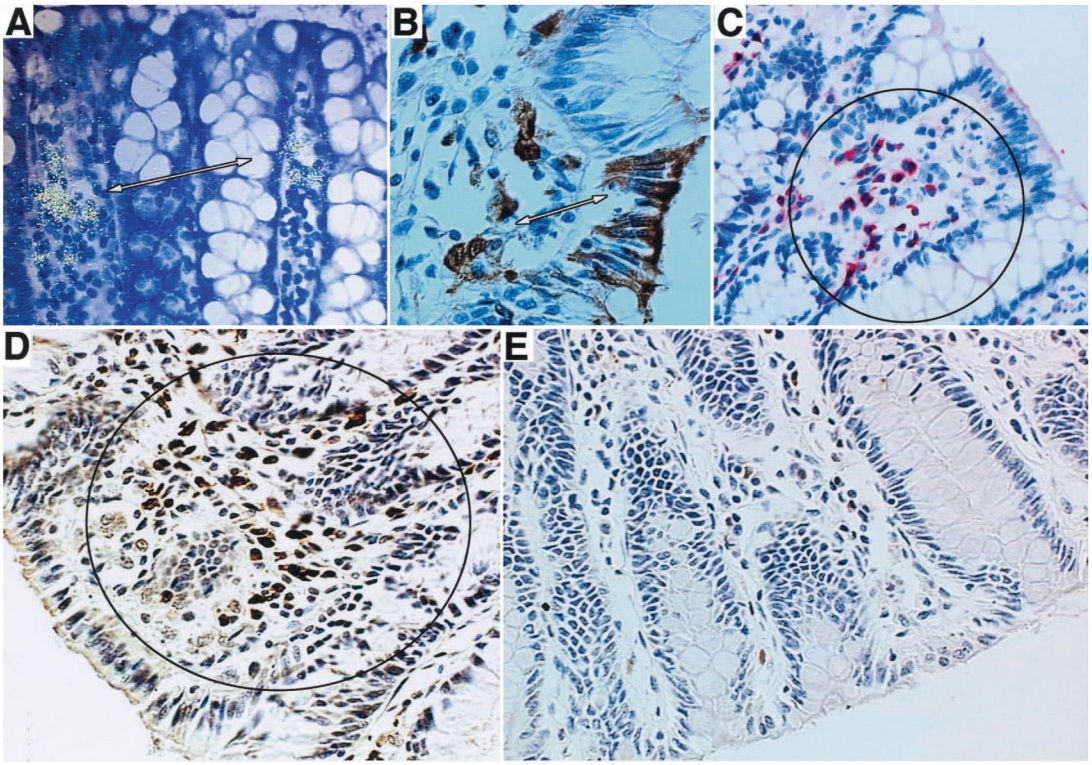

Figure 5. Virus replication and expression of Fas, Fas-L, and tumor-necrosis factor (TNF)–α in gut. Simian immunodeficiency virus (SIV) RNA$^+$ cells were detected by in situ hybridization using ^{35}S-labeled SIV-specific riboprobes, as described in Materials and Methods. In the developed radioautographs, the silver-grain signal from viral RNA imparts a white-yellow appearance to infected cells in reflected epipolarized light. *A,* SIV RNA$^+$ lamina propria cells and SIV RNA$^-$ gut epithelial cells. The double-headed arrow indicates 2 clusters of infected cells that are clearly in the lamina propria—i.e., gut epithelial cells are not productively infected. *B* and *C,* Immunohistochemical staining for Fas *(B)* and Fas-L *(C),* using substrates that impart a brown color to Fas$^+$ cells and a red color to Fas-L+ cells. The double-headed arrow in panel *B* indicates a cluster of Fas+ cells in lamina propria and overlying Fas+ gut epithelial cells in the large bowel at the onset of gut epithelial cell apoptosis, and panel *C* shows that, at that time, there are increased numbers of Fas-L$^+$ cells in lamina propria *(encircled). D* and *E,* Immunohistochemical staining for TNF-α. *D,* Encircled cluster of brown TNF-α$^+$ cells in lamina propria at the onset of gut infection. As shown in panel *E,* at peak apoptosis, 14 dpi, there are no detectable TNF- α$^+$ cells. Original magnifications, ×400.

entry [23] that has been found to be implicated in HIV enteropathy [24, 25]. Before and at the onset of gut infection in the animals, we detected only background levels of viral RNA in a particulate pattern characteristic of virions deposited along the basal surfaces of gut epithelium (figure 6*A*), and GPR15/Bob was mainly detectable at the basal surfaces of gut epithelium, to a lesser extent at apical surfaces, and in MNCs in lamina propria of the small and large bowel (figure 6*B* and 6*C*), just as has been described as occurring in human gut tissues [24]. However, at the peak of gut epithelial cell apoptosis, we observed a striking pattern of virion binding to the basal surfaces of gut epithelium in the large bowel (figure 6*D* and 6*E*) and small bowel (figure 6*F*), which coincided with a previously undescribed and remarkable transcytosis and shedding of GPR15/ Bob into the intestinal lumen (figure 6*G* and 6*H*). By 28 dpi, there were concordant decreases in gut epithelial cell apoptosis, luminal shedding of GPR15/Bob, and increased expression of the latter at the basal and apical surfaces of gut epithelium (figure 6*I*).

Discussion

The principal finding that we have reported here—that is, massive gut epithelial cell apoptosis—now provides both a mechanism for the regenerative enteropathy of early SIV infection and an explanation for the increased expression of cell-cycle genes that elsewhere have been documented in microarray studies of SIV enteropathy [9, 10]. Although the impact that this gut epithelial cell apoptosis– driven regenerative pathology has on the function of the gut mucosal barrier cannot be directly determined by studies of fixed tissues, barrier dysfunction has been documented in acute SIV infection [6], and we also observed additional evidence of histopathological changes in the gut, in the neutrophilic microabscesses at 28 dpi. As has been recently proposed, impaired function of the mucosal barrier could potentially contribute to systemic immune activation, through microbial translocation [26, 27], which would help the virus to maintain a persistent infection in the gut in 2 ways: (1) by providing activated CD4$^+$ T cell targets to sustain infection

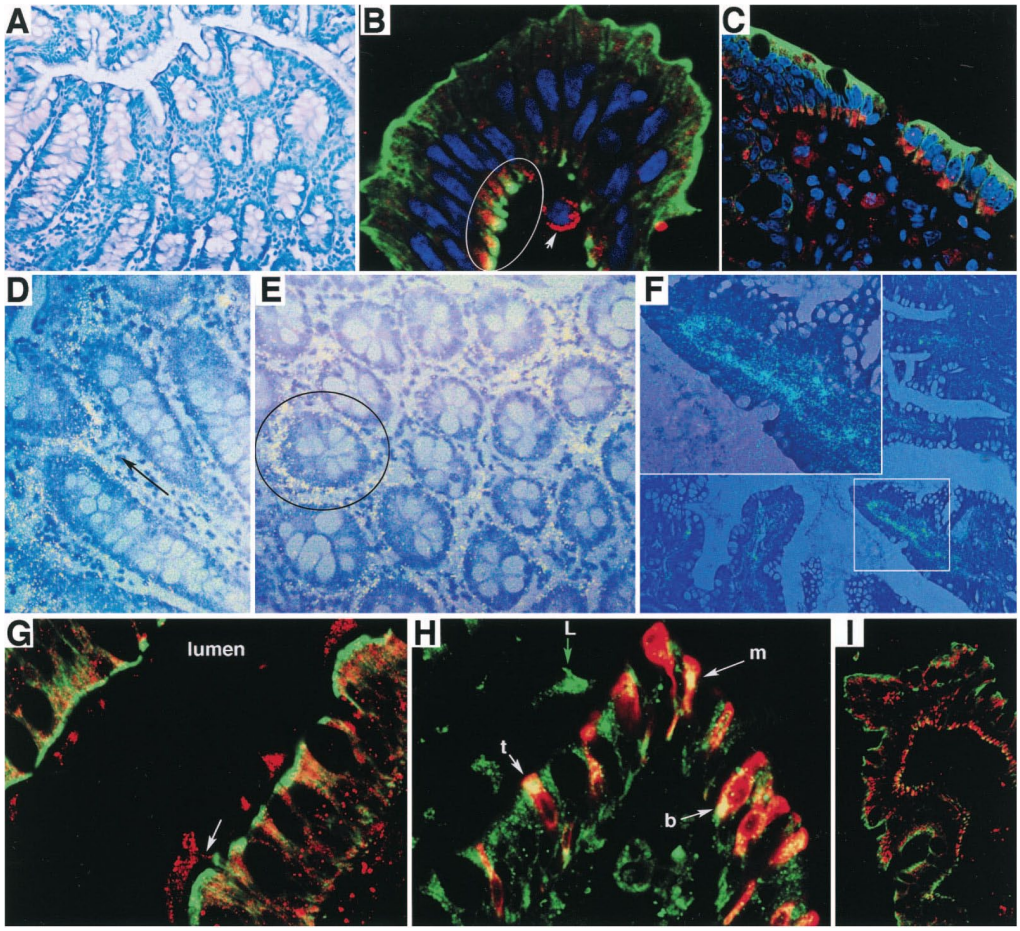

Figure 6. Virion deposition and translocation and shedding of GPR15/Bob. *A* and *D–F,* Virus association with GPR15/Bob. Viral RNA in virions was detected by in situ hybridization using ^{35}S-labeled simian immunodeficiency virus–specific riboprobes. In the developed radioautographs, the silver grains that are the signal from virion RNA have a white-yellow to bluish appearance in reflected epipolarized light. *A,* Background levels of binding in the large bowel of an uninfected animal. *D–E,* Peak apoptosis. The black arrow indicates silver grains in a particulate and diffuse pattern suggesting virion deposition along the basal surfaces of colonic crypts either oriented mainly longitudinally *(D)* or in cross-section *(E).* Original magnifications, ×200. *F,* Jejunal villi. The inset (original magnification, ×400) shows a similar pattern of virions deposited at the basal surfaces of 1 of the jejunal villi in the section. Original magnification, ×100. *B, C,* and *G–I,* Changes in pattern of localization of GPR15/Bob in small and large bowel, associated with infection and gut epithelial cell apoptosis. GPR15/Bob was stained red, and gut epithelial cells were stained green, with fluorophores and, respectively, antibodies to GPR15/Bob and to cytokeratins 5, 6, 8, 17, and 19. Nuclei were counterstained blue with TOTO-3, as described in Materials and Methods. Original magnifications, ×600. *B,* GPR15/Bob before viral replication in gut, localizing mainly to basal sides of gut epithelium *(encircled)* and to mononuclear cells in the lamina propria *(small arrow). C,* Onset of viral replication. GPR15/Bob is still concentrated at the basal side of gut epithelium. *G–H,* Transcytosis and shedding of GPR15/Bob at peak gut epithelial cell apoptosis. *G,* Vesicles of GPR15/Bob transiting the cell into the lumen. The arrow indicates connections between GPR15/Bob in the lumen and an epithelial cell. The staining for cytokeratins reveals intact gut epithelial cells below GPR15/Bob in the lumen, showing that luminal GPR15/Bob is not in shed apoptotic cells. *H,* Sections stained with antibodies and with fluorophores to GPR15/Bob *(green)* and cleaved cytokeratin 18 *(red),* as a marker for gut epithelial cell apoptosis. Colocalizing stains reveal transcytosing GPR15/Bob at the basal *(b),* middle *(m),* and top *(t)* in apoptotic gut epithelial cells. Note that GPR15/Bob in the lumen *(L) (green arrow)* is not also stained with anticleaved cytokeratin 18 and thus is not shed into the lumen in apoptotic gut epithelial cells. *I,* After peak of gut epithelial cell apoptosis. GPR15/Bob is concentrated at the basal and apical surfaces of gut epithelial cells, with little evidence of transcytosis and shedding.

and (2) by blunting the SIV-specific CD8$^+$ T cell response in the gut [28], perhaps because of a countering immunosuppressive T regulatory response, as has been shown for peripheral lymph nodes [29].

SIV infection may induce gut epithelial cell apoptosis by established as well as novel mechanisms whose relative contributions will reflect the rapidly changing dynamics of infection. At the onset of gut infection, there are rapid increases in lamina propria CD4 T cell apoptosis, which are associated with parallel increases in Fas and Fas-L expression in lamina propria T cells, which we elsewhere have proposed as being the mechanism of CD4 T cell apoptosis and the major mechanism of CD4 T cell depletion in early infection [13]. Here we have shown that there are

focal increases in Fas expression in intestinal epithelial cells (IECs) overlying foci of Fas-L$^+$ lamina propria mononuclear cells, such that gut epithelial cell apoptosis may be induced by these cells, which elsewhere has been proposed as the mechanism of enterocyte apoptosis in celiac disease [17].

Proinflammatory cytokines IFN-γ and TNF-α might also play a role in gut epithelial cell apoptosis, as they do in inflammatory bowel diseases [18, 19]. In their analysis of cytokinemRNAlevels in tissues from these animals, Abel et. al. [20] have shown that there are increased levels of these cytokines in the gut as well as in other tissues, and we have shown here that there are increased numbers of TNF-α$^+$ cells in the lamina propria at a time when IEC apoptosis is increasing. However, TNF-α and IFN-γ mRNA levels in the jejunum were actually lower than either those in uninfected control animals or those in infected animals before gut infection [20], so these cytokines cannot account for gut epithelial cell apoptosis in both small and large bowel.

Fas and Fas-L and cytokines also cannot be the principal mechanism underlying peak gut epithelial cell apoptosis. We have shown that there are few Fas-L$^+$ cells in the lamina propria at 14 dpi, a finding that reflects the massive depletion of CD4 T cells by this time. There are also few TNF-α$^+$ cells at 14 dpi, which is in good agreement with the cytokinemRNA-data showing decreased mRNA levels at 14 dpi [20].

On the basis of both the observed striking focal deposition of virus and the coincident changes, at the peak of gut epithelial cell apoptosis, in the expression and location in gut epithelial cellassociated GPR15/Bob-IECs, we speculate that peak apoptosis might be the result of virotoxic effects that virion gp120 has on gut epithelial cells. In a previous study, such a virotoxic mechanism has been proposed to account for both the loss of microtubules and the increased paracellular permeability observed in vitro, which were the virotoxic effects of exposing cultured colonic cells to HIV-1 gp120 [24]. Because apoptosis was not observed in that previous in vitro study, we propose that IEC apoptosis in vivo is the result of what we have reported here—that is, the demonstrable effect that much higher local concentrations of virion-associated gp120 has on GPR15/Bob expression in gut epithelial cells, an effect that could trigger massive signaling and consequent apoptosis and observed changes in GPR15/Bob. The predisposition of terminally differentiated IECs to undergo apoptosis as they near the luminal surface [30] is a necessary second component of this speculative model, to explain the restriction of apoptosis when virus is deposited at the basal surfaces of gut epithelial cells along the villi and crypts (figure 6).

The discovery of gut epithelial cell apoptosis as the underlying mechanism of the regenerative pathology of early infection was the result of very close examination of tissues collected [12] in the stunningly fast phase of a slow infection, in which the most dramatic events unfold over a period of 7 days. Thus, the power of this highly relevant nonhuman primate model of HIV-1 infection is to enable studies of pathogenic mechanisms that, by extension, may apply to HIV-1 infection in humans but than cannot be studied in humans because the time frame in which they are most evident precedes the earliest time when HIV-1–infected individuals present with the symptoms of acute retroviral infection [13, 31–33]. The speed with which SIV induces apoptosis of both CD4 T cell populations and the intestinal epithelium, with consequent pathological damage to the gut mucosa, attests to the need for new approaches to early interventions to prevent or greatly moderate the deleterious consequences that infection has on adaptive and innate host defenses.

Acknowledgments – We thank Christopher Miller, Zhongmin Ma, Tracy Rourke, and Katherine Lantz (all of the California National Primate Research Center) for assistance and Tim Leonard and Colleen O'Neill for help in preparing the figures and manuscript. This work was supported by grants from the National Center for Research Resources, Public Health Services (grant U51 RR00169 to California National Primate Research Center); National Institute of Allergy and Infectious Diseases (R01 grant AI48484 to A.T.H. and grants AI51239 and AI51596 to Christopher Miller).

References

1. Kotler DP, Gaetz HP, Lange M, Klein EB, Holt PR. Enteropathy associated with the acquired immunodeficiency syndrome. *Ann Intern Med* 1984; 101:421–8.
2. Ullrich R, Zeitz M, Heise W, L'Age M, Hoffken G, Riecken EO. Small intestinal structure and function in patients infected with human immunodeficiency virus (HIV): evidence for HIV-induced enteropathy. *Ann Intern Med* 1989; 111:15–21.
3. Kotler DP, Reka S, Borcich A, Cronin WJ. Detection, localization, and quantitation of HIV-associated antigens in intestinal biopsies from patients with HIV. *Am J Pathol* 1991; 139:823–30.
4. Kotler DP. HIV infection and the gastrointestinal tract. *AIDS* 2005; 19: 107–17.
5. Heise C, Vogel P, Miller CJ, Halsted CH, Dandekar S. Simian immunodeficiency virus infection of the gastrointestinal tract of rhesus macaques: functional, pathological, and morphological changes. *Am J Pathol* 1993; 142:1759–71.
6. Heise C, Miller CJ, Lackner A, Dandekar S. Primary acute simian immunodeficiency virus infection of intestinal lymphoid tissue is associated with gastrointestinal dysfunction. *J Infect Dis* 1994; 169:1116–20.
7. Kewenig S, Schneider T, Hohloch K, et al. Rapid mucosal CD4(+) T-cell depletion and enteropathy in simian immunodeficiency virus-infected rhesus macaques. *Gastroenterology* 1999; 116:1115–23.
8. Kotler DP, Shimada T, Snow G, et al. Effect of combination antiretroviral therapy upon rectal mucosal HIV RNA burden and mononuclear cell apoptosis. *AIDS* 1998; 12:597–604.
9. George MD, Sankaran S, Reay E, Gelli AC, Dandekar S. Highthroughput gene expression profiling indicates dysregulation of intestinal cell cycle mediators and growth factors during primary simian immunodeficiency virus infection. *Virology* 2003; 312:84–94.

10. George MD, Reay E, Sankaran S, Dandekar S. Early antiretroviral therapy for simian immunodeficiency virus infection leads to mucosal CD4+ T-cell restoration and enhanced gene expression regulating mucosal repair and regeneration. *J Virol* 2005; 79:2709 –19.
11. Zeitz M, Ullrich R, Schneider T, Kewenig S, Hohloch K, Riecken EO. HIV/SIV enteropathy. *Ann NY Acad Sci* 1998; 859:139–48.
12. Miller CJ, Li Q, Abel K, et al. Propagation and dissemination of infection after vaginal transmission of SIV. *J Virol* 2005; 79:9217–27.
13. Li Q, Duan L, Estes JD, et al. Peak SIV replication in resting memory CD4(+) T cells depletes gut lamina propria CD4(+) T cells. *Nature* 2005; 434:1148 –52.
14. Holubec H, Payne CM, Bernstein H, et al. Assessment of apoptosis by immunohistochemical markers compared to cellular morphology in ex vivo-stressed colonic mucosa. *J Histochem Cytochem* 2005; 53:229–35.
15. Radtke F, Clevers H. Self-renewal and cancer of the gut: two sides of a coin. *Science* 2005; 307:1904–9.
16. Sakai T, Kimura Y, Inagaki-Ohara K, Kusugami K, Lynch DH, Yoshikai Y. Fas-mediated cytotoxicity by intestinal intraepithelial lymphocytes during acute graft-versus-host disease in mice. *Gastroenterology* 1997; 113:168–74.
17. Ciccocioppo R, Di Sabatino A, Parroni R, et al. Increased enterocyte apoptosis and Fas-Fas ligand system in celiac disease. *Am J Clin Pathol* 2001; 115:494 –503.
18. Guy-Grand D, DiSanto JP, Henchoz P, Malassis-Seris M, Vassalli P. Small bowel enteropathy: role of intraepithelial lymphocytes and of cytokines (IL-12, IFN-gamma, TNF) in the induction of epithelial cell death and renewal. *Eur J Immunol* 1998; 28:730–44.
19. Piguet PF, Vesin C, Donati Y, Barazzone C. TNF-induced enterocyte apoptosis and detachment in mice: induction of caspases and prevention by a caspase inhibitor, ZVAD-fmk. *Lab Invest* 1999; 79:495–500.
20. Abel K, Rocke DM, Chohan B, Fritts L, Miller CJ. Temporal and anatomic relationship between virus replication and cytokine gene expression after vaginal simian immunodeficiency virus infection. *J Virol* 2005; 79:12164 –72.
21. Chen Z, Zhou P, Ho DD, Landau NR, Marx PA. Genetically divergent strains of simian immunodeficiency virus use CCR5 as a coreceptor for entry. *J Virol* 1997; 71:2705–14.
22. Choe H, Farzan M, Konkel M, et al. The orphan seven-transmembrane receptor apj supports the entry of primary T-cell-line-tropic and dualtropic human immunodeficiency virus type 1. *J Virol* 1998; 72:6113– 8.
23. Edinger AL, Mankowski JL, Doranz BJ, et al. CD4-independent, CCR5- dependent infection of brain capillary endothelial cells by a neurovirulent simian immunodeficiency virus strain. *Proc Natl Acad Sci USA* 1997; 94:14742–7.
24. Clayton F, Kotler DP, Kuwada SK, et al. Gp120-induced Bob/GPR15 activation: a possible cause of human immunodeficiency virus enteropathy. *Am J Pathol* 2001; 159:1933–9.
25. Maresca M, Mahfoud R, Garmy N, Kotler DP, Fantini J, Clayton F. The virotoxin model of HIV-1 enteropathy: involvement of GPR15/Bob and galactosylceramide in the cytopathic effects induced by HIV-1 gp120 in the HT-29-D4 intestinal cell line. *J Biomed Sci* 2003; 10:156–66.
26. Brenchley JM, Price DA, Douek DC. HIV disease: fallout from a mucosal catastrophe? *Nat Immunol* 2006; 7:235–9.
27. Brenchley JM, Price DA, Schacker TW, et al. Microbial translocation is a cause of systemic immune activation in chronic HIV infection. *Nat Med* 2006; 12:1365–71.
28. Reynolds MR, Rakasz E, Skinner PJ, et al.CD8+ T-lymphocyte response to major immunodominant epitopes after vaginal exposure to simian immunodeficiency virus: too late and too little. *J Virol* 2005; 79:9228–35.
29. Estes JD, Li Q, Reynolds MR, et al. Premature induction of an immunosuppressive regulatory T cell response during acute simian immunodeficiency virus infection. *J Infect Dis* 2006; 193:703–12.
30. Grossmann J, Walther K, Artinger M, Rummele P, Woenckhaus M, Scholmerich J. Induction of apoptosis before shedding of human intestinal epithelial cells. *Am J Gastroenterol* 2002; 97:1421–8.
31. Haase AT. Perils at mucosal front lines for HIV and SIV and their hosts. *Nat Rev Immunol* 2005; 5:783–92.
32. Mattapallil JJ, Douek DC, Hill B, Nishimura Y, Martin M, Roederer M. Massive infection and loss of memory CD4(+) T cells in multiple tissues during acute SIV infection. *Nature* 2005; 434:1093–7.
33. Pope M, Haase AT. Transmission, acute HIV-1 infection and the quest for strategies to prevent infection. *Nat Med* 2003; 9:847–52.

Table 2. Details on antibodies used.

Antibody/reagent	Clone/catalog no.	Tissue fixation	Antigen-retrieval pretreatment	Antibody dilution	Manufacturer	Address
Apoptotic/CK18 marker (kit)	Catalog no. CM224-KIT, clone BC/M30	4% Paraformaldehyde	Reveal water bath for 15 min at 95°C–98°C	1:100	Biocare Medical	San Jose, CA 95131–1807
Active caspase-3	(5A1) Rabbit mAB	4% Paraformaldehyde	Decloaker water bath for 20 min at 95°C–98°C	1:300	Cell Signaling Technology	3 Trask Ln., Danvers, MA 01923
Active caspase-3	Ab-2 (rabbit antihuman)	4% Paraformaldehyde	1 mmol/L EDTA, pH 8.0; water bath for 10 min at 95°C–98°C	1:100	Oncogen Research Product	10394 Pacific Center Ct. San Diego, CA 92121
Active caspase-3	Rabbit mAB p17, catalog no. 1476–1	4% paraformaldehyde	Decloaker water bath for 20 min at 95°C–98°C	1:100	Epitomics	Epitomics, Inc., 863 Mitten Rd., Ste. 103, Burlingame, CA 94010–1303
GPR15/Bob	Rabbit pAB antihuman, catalog no. ab12543	Streck tissue fixative	1 mmol/L EDTA, pH 8.0; water bath for 10 min at 95°C–98°C	1:100	Abcam, Inc.	1 Kendall Square, Ste. 341, Cambridge, MA 02139–1517
BCL2	Mouse mAB 100/D5	4% Paraformaldehyde	1 mmol/L EDTA, pH 8.0; water bath for 10 min at 95°C–98°C	1:25	Abcam, Inc.	1 Kendall Square, Ste. 341, Cambridge, MA 02139–1517
CCR5	3A9	Streck tissue fixative	10 mmol/L sodium citrate, pH 6.0; water bath for 15 min at 95°C–98°C	1:100	BD Biosciences	2350 Qume Dr., San Jose, CA 95131
Fas	Mouse mAB antihuman CD95, APO-1/Fas, clone APO-1	Streck tissue fixative	10 mmol/L sodium citrate, pH 6.0; water bath for 15 min at 95°C–98°C	1:50	DakoCytomation California, Inc.	Dako North America, Inc. 6392 Via Real, Carpinteria, CA 93013
Fas	Mouse mAB clone GM30	Streck tissue fixative	1 mmol/L EDTA, pH 8.0; water bath for 10 min at 95°C–98°C	1:300	Vector Laboratories, Inc.	30 Ingold Rd., Burlingame, CA 94010
Fas	Pc69 Ab-1 (rabbit pAB)	4% paraformaldehyde	1 mmol/L EDTA, pH 8.0; water bath for 10 min at 95°C–98°C	1:100	Calbiochem	EMD Biosciences, Inc. 10394 Pacific Center Ct., San Diego, CA 92121
Fas-L	CN-20 (rabbit antihuman)	Streck tissue fixative	10 mmol/L sodium citrate, pH 6.0; water bath for 10 min at 95°C–98°C	1:100	Santa Cruz Biotechnology, Inc.	2145 Delaware Ave., Santa Cruz, CA 95060
Fas-L	G247–4	Streck tissue fixative	Decloaker water bath for 20 min at 95°C–98°C	1:300	BD Pharmingen	2350 Qume Dr., San Jose, CA 95131–1807
Fas-L	Mike-1, rat pAB	Streck tissue fixative	1 mmol/L EDTA, pH 8.0; water bath for 10 min at 95°C–98°C	1:200	Abcam	One Kendall Square, Bldg. 200, 3rd Fl., Cambridge, MA 02139
Galetin	Rabbit pAB, catalog no: 500-P210	Streck tissue fixative	1 mmol/L EDTA, pH 8.0; water bath for 10 min at 95°C–98°C	1:200	PeproTech, Inc.	Princeton Business Park, 5 Crescent Ave., P.O. Box 275, Rocky Hill, NJ 08553

Ki67	MM1 monoclonal	4% paraformaldehyde	10 mmol/L sodium citrate, pH 6.0; water bath for 10 min at 95°C–98°C	1:100	Vector Laboratories, Inc.	30 Ingold Rd., Burlingame, CA 94010
Cytokeratin	Mouse mAB anti-Human, cytokeratin, clone MNF116	Streck tissue fixative	1 mmol/L EDTA, pH 8.0; water bath for 10 min at 95°C–98°C	1:100	DakoCytomation California, Inc.	Dako North America, Inc., 6392 Via Real, Carpinteria, CA 93013
Mark-6 (mouse mAB anti-cytokeratin cocktail)	Catalog no. 28–0001	4% Paraformaldehyde pH 6.0; water bath for 15	10 mmol/L sodium citrate, min at 95°C–98°C	1:100 Invitrogen	Zymed Lab., PO Box 6482 Immunodetection	1600 Faraday Ave., Carlsbad, CA 92008
XIAP	mAB, clone 48	4% Paraformaldehyde	10 mmol/L sodium citrate, pH 6.0; water bath for 15 min at 95°C–98°C	1:200	BD Biosciences	2350 Qume Dr., San Jose, CA 95131
Alexa Fluor 488 donkey anti-mouse IgG	Catalog no. A21202			1:500	Molecular Probe, Invitrogen Corp.	1600 Faraday Ave. PO Box 6482, Carlsbad, CA 92008
Alexa Fluor 555 donkey anti-mouse IgG	Catalog no. A31570			1:500	Molecular Probe, Invitrogen Corp.	1601 Faraday Ave., PO Box 6482, Carlsbad, CA 92008
Alexa Fluor 488 donkey anti-rabbit IgG	Catalog No. A21206			1:500	Molecular Probe, Invitrogen Corp.	1602 Faraday Ave., PO Box 6482, Carlsbad, CA 92008
Alexa Fluor 555 donkey anti-rabbit IgG	Catalog no. A31572			1:500	Molecular Probe, Invitrogen Corp.	1603 Faraday Ave., PO Box 6482, Carlsbad, CA 92008
Detection system/blocking reagent						
DakoCytomation EnVision + System-HRP	Catalog no. K4006				DakoCytomation California, Inc.	6392 Via Real, Carpinteria, CA 93013
EDTA Decloaker	Catalog no. CB917L				Biocare Medical	4040 Pike Ln., Concordia, CA 94520–1227
Vulcan Fast Red	Chromgen system, catalog no. FR803M				Biocare Medical	4040 Pike Ln., Concordia, CA 94520–1227
March3 mouse-probe Alk Phos polymer	Catalog no. M3M532H				Biocare Medical	4040 Pike Ln., Concordia, CA 94520–1227
March3 rabbit-probe HRP-polymer	Catalog no. M3M530H				Biocare Medical	4040 Pike Ln., Concordia, CA 94520–1227
March3 mouse-HRP-polymer	Catalog no. M3M530H				Biocare Medical	4040 Pike Ln., Concordia, CA 94520–1227
Heat Retrieval-Reveal	Catalog no. RV1000M				Biocare Medical	4040 Pike Ln., Concordia, CA 94520–1227
K.5 Ilford emulsion	Catalog no. 135 5136				Polysciences, Inc.	400 Valley Rd., Warrington, PA 18976

HRP, horseradish peroxidase; mAB, monoclonal antibody; pAB, polyclonal antibody.